Ab initio study of the elastic anomalies in Pd-Ag alloys

E. K. Delczeg-Czirjak,[1] L. Delczeg,[1] M. Ropo,[1,2,3] K. Kokko,[2] M. P. J. Punkkinen,[2] B. Johansson,[1,4,5] and L. Vitos[1,4,6]
[1]*Department of Materials Science and Engineering, Applied Materials Physics, Royal Institute of Technology, SE-100 44 Stockholm, Sweden*
[2]*Department of Physics and Astronomy, University of Turku, FIN-20014 Turku, Finland*
[3]*Department of Information Technology, Åbo Akademi, FIN-20500 Turku, Finland*
[4]*Department of Physics and Materials Science, Division for Materials Theory, Uppsala University, SE-75121 Uppsala, Sweden*
[5]*School of Physics and Optoelectronic Technology and College of Advanced Science and Technology, Dalian University of Technology, Dalian 116024, China*
[6]*Research Institute for Solid State Physics and Optics, H-1525 Budapest, P.O. Box 49, Hungary*
(Received 14 November 2008; revised manuscript received 14 January 2009; published 11 February 2009)

Ab initio total-energy calculations, based on the exact muffin-tin orbital method, are used to determine the elastic properties of $Pd_{1-x}Ag_x$ random alloys in the face-centered-cubic crystallographic phase. The compositional disorder is treated within the coherent-potential approximation. The single crystal and polycrystalline elastic constants and the Debye temperature are calculated for the whole range of concentration, $0 \leq x \leq 1$. It is shown that the variation in the elastic parameters of Pd-Ag alloys with chemical composition strongly deviates from a simple linear or parabolic trend. The complex electronic origin of these anomalies is demonstrated.

DOI: 10.1103/PhysRevB.79.085107 PACS number(s): 71.15.Nc, 62.20.D−, 71.20.Be, 81.05.Bx

I. INTRODUCTION

Although the Pd-Ag alloys are commonly used in many technological applications, the behavior of their elastic properties as a function of chemical composition has not yet been established. At first glance, we might ascribe this deficiency to the apparent simplicity of the system, which suggests a smooth linear dependence for the elastic constants. However, a careful survey of the available experimental data for the equilibrium lattice parameters[1] indicates that there are at least two distinctly dissimilar regimes with slightly different slopes as a function of composition (Fig. 1). The slope change around 60%–70% Ag is anomalous and signals the presence of a transition. In mid 1990s Bruno *et al.*[2,3] presented a comprehensive theoretical study of the Fermi-surface geometry for random Pd-Ag alloys. These authors identified five distinct electronic topological transitions (ETTs) (Ref. 4) for Ag concentrations between 6% and 70%. They argued that the observed ETTs should be reflected in several physical properties, which was confirmed in the case of the equilibrium volume and mixing enthalpy using the *ab initio* Korringa-Kohn-Rostoker (KKR) coherent-potential approximation method.[2] At that time, however, it was impossible to carry out a more accurate theoretical study as a function of chemical composition and thus to reveal the footprint of the ETTs on other important equilibrium bulk parameters.

Here we present a systematic study of the elastic properties of Pd-Ag binaries using the exact muffin-tin orbital (EMTO) method.[5–9] The EMTO method is an *ab initio* tool based on density-functional theory,[10,11] which was shown to be suitable to compute the anisotropic lattice distortions and thus the elastic constants in random alloys.[9,12–18] Our primary aim is to produce consistent and accurate theoretical data, which can be used to trace the anomalies driven by the ETTs and also to serve as a starting point for future experimental investigations. To this end, we select the recently developed Perdew-Burke-Ernzerhof exchange-correlation approximation revised for metallic bulk and surface systems (PBEsol),[19] which yields accurate equation of state (equilibrium volume and bulk modulus) for pure Pd and Ag,[20] as well as for the Pd-Ag system (see Sec. III).

According to the experimental phase diagram, Pd and Ag form continuous solid solution within the face-centered-cubic (fcc) crystallographic phase.[21] Hence, in the present study we use a random fcc solid solution to describe the Pd-Ag system. Nevertheless, theoretical calculations by Müller and Zunger[22] showed that ordering in Pd-Ag occurs at temperatures (T) below ~340 K in Ag-rich alloys and ~270 K in Pd-rich alloys. A similar ordering tendency was predicted by Ruban *et al.*[23] in their calculations based on the screened generalized perturbation method. In light of these theoretical findings, our results obtained for random alloys are expected to be approximately valid at temperatures

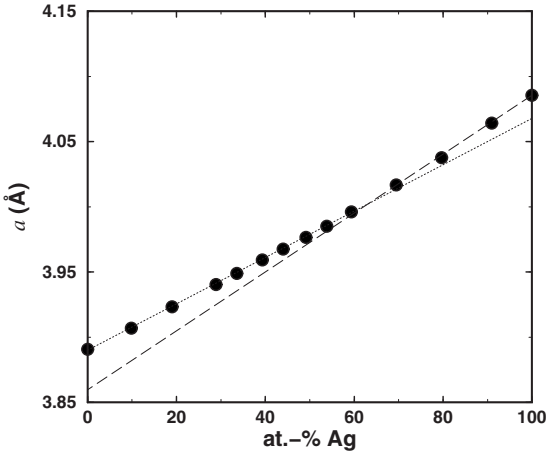

FIG. 1. Experimental equilibrium lattice parameters for Pd-Ag alloys plotted as a function of Ag concentration (Ref. 1). The dotted and dashed lines are linear fits to two distinct regimes corresponding to alloys with Ag concentration between 0%–60% and 60%–100%, respectively.

around and above the room temperature. On the other hand, it is well known that the elastic constants of Ag follow the normal decreasing trend with increasing temperature,[24] whereas those of Pd exhibit anomalous temperature dependence (e.g., c_{44} increases with T above ~ 100 K).[25] In Pd-Ag system, similarly to the Nb-Zr system,[18,26] the above anomaly should gradually diminish with increasing Ag content. The difference in the temperature factors for the elastic constants of Pd and Ag brings another uncertainty to our theoretical results. Therefore, in addition to the fundamental approximations (see Sec. II), the neglected effects due to ordering and anomalous temperature factors in Pd-rich alloys should also be taken into account when the present theoretical results are to be compared with future experimental data.

Using the EMTO-PBEsol approach, we calculate the single crystal and polycrystalline elastic moduli $[c(x)]$ of $Pd_{1-x}Ag_x$ alloys as a function of concentration x. We show that despite the fact that the calculations are carried out for a single phase, within which both end members are thermodynamically and mechanically stable, the variation in the elastic parameters with concentration follows anomalous trends. Namely, all the theoretical $c(x)$ curves deviate strongly from a simple linear behavior. The deviations are different, and the largest deviations and the first-order discontinuities occur at different concentrations. Our findings also confirm the complex electronic structure origin of the above elastic anomalies in Pd-Ag alloys.

The rest of this paper is divided in two main sections and conclusions. Section II presents the theoretical tools. This includes a brief overview of the elastic properties and the *ab initio* electronic structure method, and the most important details of the numerical calculations. The results are presented and discussed in Sec. III.

II. THEORETICAL TOOL

A. Elastic properties

The elastic properties of single crystals are described by the elements c_{ij} of the elasticity tensor. For a cubic lattice there are three independent elastic constants, c_{11}, c_{12}, and c_{44}. They are connected to the bulk modulus $B=(c_{11}+2c_{12})/3$ and tetragonal shear modulus $c'=(c_{11}-c_{12})/2$.

The main difference between single-crystal alloys and real materials is the inherent disorder. The most common form of disorder is the breakdown of the long-range order of the crystal lattice sites. Most of the real solid materials have a hierarchy of structures beginning with atoms and ascends through various nanometer or micrometer level crystalline grains. The misoriented single crystals are separated by stacking faults, interphase boundaries, etc. The only way to establish the elastic parameters of these polycrystalline systems is to first derive data for single crystals and then to transform these data to macroscopic quantities using suitable averaging methods based on statistical mechanics. On a large scale, a polycrystalline material can be considered as quasi-isotropic or isotropic, and it is completely described by the bulk modulus B and the shear modulus G. For a cubic lattice the polycrystalline bulk modulus is identical with the single-crystal bulk modulus. For the shear modulus we adopt the arithmetic Hill average $G=(G_R+G_V)/2$ (see, e.g., Ref. 9), where the Reuss and Voigt bounds are given in terms of single-crystal elastic constants, viz.,

$$G_R = 5(c_{11}-c_{12})c_{44}(4c_{44}+3c_{11}-3c_{12})^{-1} \quad (1)$$

and

$$G_V = (c_{11}-c_{12}+3c_{44})/5. \quad (2)$$

The Young modulus E and the Poisson ratio ν are connected to B and G by the relations $E=9BG/(3B+G)$ and $\nu=(3B-2G)/(6B+2G)$. The longitudinal sound velocity is related to B and G, viz., $\rho v_L^2=B+(4G)/3$, whereas the transversal velocity depends only on G, viz., $\rho v_T^2=G$. In these expressions ρ is the density. Using the average sound velocity given by $3v_m^{-3}=v_L^{-3}+2v_T^{-3}$, we obtain the elastic Debye temperature for a polycrystalline material as

$$\Theta = (\hbar/k_B)(6\pi^2/V)^{1/3}v_m, \quad (3)$$

where V is the average atomic volume, and $\hbar$ and k_B are Planck's and Boltzmann's constants, respectively.

B. Total-energy method

A full description of the EMTO theory and the corresponding method may be found in Refs. 5–9. Within this approach the compositional disorder is treated using the coherent-potential approximation[27,28] and the total energy is computed via the full charge-density technique.[29]

The EMTO theory formulates an efficient and accurate method of solving the Kohn-Sham equation.[11] For simplicity, it may be considered as an improved KKR method, where the exact Kohn-Sham potential is represented by large overlapping potential spheres. Inside these spheres the potential is spherically symmetric and constant between the spheres. However, within the EMTO theory, in contrast to the usual muffin-tin-based methods, the one-electron states are determined exactly (within the common numerical errors) for an optimized overlapping muffin-tin potential. This potential is chosen as the best possible spherical approximation to the exact potential;[6,9,30] the radii of the potential spheres, the spherical potential waves, and the constant value from the interstitial are calculated by minimizing (a) the deviation between the exact and overlapping potentials and (b) the errors coming from the overlap between spheres. The accuracy of the EMTO method for the equation of state and elastic properties of metals and disordered alloys has been demonstrated in a number of former works.[8,9,12–18]

C. Details of the numerical calculations

Bruno *et al.*[3] pointed out that the ETT at 0.35% Ag has a relativistic origin. Nevertheless, in the present work we adopted the scalar-relativistic approximation instead of a fully relativistic study. The latter would require a significantly larger computational effort without changing the basic physics around the most important ETTs at 53% and 70% Ag. The one-electron equations were solved within soft-core approximations. The Green's function was calculated for 16 complex energy points distributed exponentially on a semi-

circular contour. In the basis set we included s, p, d, and f orbitals, and in the one-center expansion of the full charge density we used the cutoff $l^h_{\max}=8$. The electrostatic correction to the single-site coherent-potential approximation was described using the original screened impurity model[31] with a screening parameter of 0.9.

The cubic elastic constants of $Pd_{1-x}Ag_x$ alloys were calculated as a function of the chemical composition for the concentration range $0 \le x \le 1$. At each concentration x the theoretical equilibrium lattice parameter a and the bulk modulus B were determined from a Murnaghan equation of state[32] fitted to the *ab initio* total energies of fcc structures for 17 different atomic volumes. In order to calculate the two cubic shear moduli c' and c_{44} we used the following volume conserving orthorhombic and monoclinic deformations:

$$\begin{pmatrix} 1+\varepsilon_o & 0 & 0 \\ 0 & 1-\varepsilon_o & 0 \\ 0 & 0 & \dfrac{1}{(1-\varepsilon_o)^2} \end{pmatrix} \quad \text{and} \quad \begin{pmatrix} 1 & \varepsilon_m & 0 \\ \varepsilon_m & 1 & 0 \\ 0 & 0 & \dfrac{1}{1-\varepsilon_m^2} \end{pmatrix}, \tag{4}$$

respectively, applied on the conventional cubic unit cell. The corresponding distorted structures were described as face-centered-orthorhombic and body-centered-orthorhombic lattices, respectively. The total energies, $E(\varepsilon_o)=E(0)+2Vc'\varepsilon_o^2+O(\varepsilon_o^4)$ and $E(\varepsilon_m)=E(0)+2Vc_{44}\varepsilon_m^2+O(\varepsilon_m^4)$ were computed for six distortions $\epsilon=0.00, 0.01, \ldots, 0.05$. To obtain the accuracy needed for the calculation of elastic constants in the irreducible wedge of the Brillouin zones we used 20 000–27 000 k points, depending on the particular distortion.

The self-consistent EMTO calculations were performed within the local-density approximation (LDA) (Ref. 33) for the exchange-correlation functional. In order to be able to commit ourselves to a particular exchange-correlation approximation, first we need to investigate the accuracy of different density-functional approximations for the Pd-Ag system. To this end, in addition to the LDA, the total energy was also calculated using the Perdew-Burke-Ernzerhof (PBE) generalized gradient approximation,[34] the recent PBE approximation revised for solids and solid surfaces (PBEsol),[19] the local airy gas (LAG) approximation,[35] and the AM05 approximation.[36] It has been shown that the above perturbative treatment of the gradient corrected approximations introduces errors which are below the typical numerical errors associated with such calculations.[20,37]

III. RESULTS

A. Assessing the accuracy

It has already been shown that the EMTO method gives equation of states for Pd and Ag in excellent agreement with the most accurate full-potential method.[9] A similar comparison in the case of Pd-Ag solid solutions is not possible since there is no accurate theoretical data available. Instead, here we use our calculated equilibrium lattice parameters and bulk moduli to assess the accuracy of different density-functional approximations. Figure 2 (lower panel) shows that

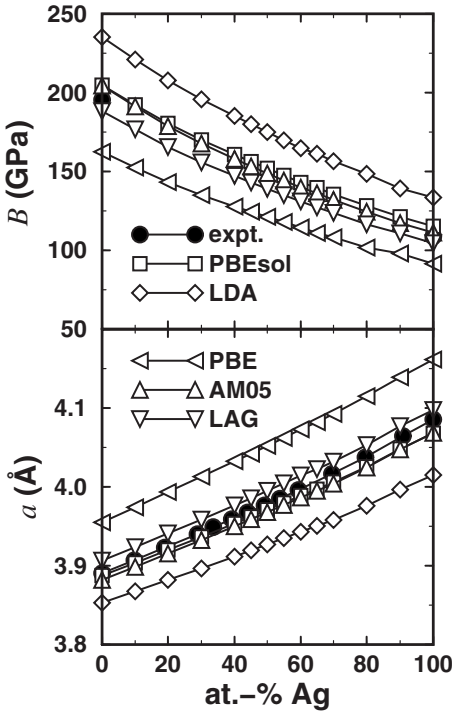

FIG. 2. Concentration dependence of the present theoretical (LDA, PBE, PBEsol, LAG, and AM05) and experimental lattice constants (a) (lower panel) and bulk moduli (B) (upper panel) for fcc Pd-Ag random alloys. The experimental data are from Ref. 1 for a and Refs. 38 and 39 for B.

LDA underestimates and PBE overestimates the lattice parameters of Pd-Ag alloys, whereas the PBEsol, LAG, and AM05 values follow closely the experimental curve. In particular, the recent PBEsol approximation reproduces the experimental equilibrium volumes with high accuracy. The relative performance of the five considered functionals is also reflected in the calculated bulk moduli (Fig. 2, upper panel). For B the best agreement between theory and experiment is obtained for the LAG approximation. However, in lack of the experimental bulk moduli for the solid solutions, our final verdict on the exchange-correlation approximations has to be based on the lattice parameter only. Henceforth, since for the lattice-parameter PBEsol yields marginally better results than AM05 and LAG, the elastic constants in the present work have been obtained by means of the PBEsol exchange-correlation functional.

To establish the accuracy of the EMTO-PBEsol approach for the single-crystal elastic constants, in Fig. 3 we compare the present results for Pd and Ag with the available experimental data[38,39] as well as with former theoretical values. The figure is explained in details in the caption and the text below. The full-potential linearized augmented plane-wave (FLAPW) results[40] for Pd are shown for both LDA and PBE, whereas the full-potential linear muffin-tin orbitals (FPLMTO) results[41] for Pd and Ag are shown for LDA only. Note that a perfect correspondence between the four different sets of data would result in symbols lying on the 1:1 line. For Ag, the agreement among the EMTO, FPLMTO, and experimental results is good. For Pd, we can observe large deviations in the case of the EMTO values for c_{44} and E, the

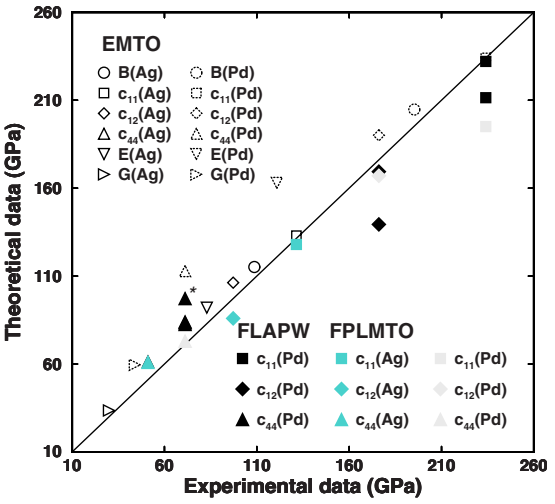

FIG. 3. (Color online) Present theoretical elastic constants (EMTO, open symbols) for pure Pd and Ag compared to the available experimental (Refs. 38 and 39) and former theoretical values. The EMTO calculations were done using the PBEsol approximation. The two sets of FLAPW results (Ref. 40) for Pd (black filled symbols) were obtained using the LDA (larger values) and PBE (smaller values) approximations. The triangle with star is a second FLAPW-PBE result for c_{44} obtained using a different lattice distortion (see text). The FPLMTO results (Ref. 41) (Ag dark gray and Pd light gray) were obtained using LDA. Note that the FLAPW-LDA and FLAPW-PBE values for c_{44}(Pd) and the FPLMTO and EMTO values for c_{44}(Ag) overlap. For completeness, the EMTO values for the bulk, Young's, and shear moduli are also compared to the corresponding experimental data.

FLAPW-PBE values for c_{11} and c_{12}, and the FPLMTO value for c_{11}. Jona and Marcus[40] used two different distortions to compute the elastic constant c_{44} for Pd. We note that, apart from the numerical inaccuracies, the two values of c_{44} obtained from these two FLAPW calculations should be identical. However, the reported large (~15 GPa) difference (Fig. 3, black filled triangles with and without star) illustrates the numerical difficulties associated with such calculations. We speculate that the large error in EMTO c_{44}(Pd) [and E(Pd)] has similar numerical origin. The low FLAPW-PBE values for c_{11} and c_{12} from Fig. 3 are not surprising, since PBE strongly overestimates the equilibrium volume of Pd and thus underestimates the elastic constants. The large deviation reported in FPLMTO calculation of c_{11}(Pd) is less clear. On the other hand, the EMTO values for both c_{11}(Pd) and c_{12}(Pd) are in good agreement with experiment. The overall good agreement between our and former theoretical results, and between the present theoretical and the available experimental data qualify for using the EMTO-PBEsol approach to establish the compositional dependence of the elastic properties of Pd-Ag alloys.

B. Composition dependence of the elastic parameters

The calculated single crystal and polycrystalline elastic moduli as well as the polycrystalline Debye temperature of Pd-Ag random alloys are listed in Table I and also plotted in Fig. 4 as a function of Ag concentration. Since there are no other theoretical and experimental data available, the panels on this figure display only the present EMTO-PBEsol results. Note that the ordinates for the single-crystal elastic constants and the bulk modulus are identical. On these scales, $c_{ij}(x)$ and $B(x)$ follow a nearly linear trend. The situation is quite different for the polycrystalline elastic moduli $E(x)$, $G(x)$, and $\nu(x)$ and also for the Debye temperature $\Theta(x)$. In particular, the Poisson ration exhibits a nonmonotonous behavior with a marked minimum between 50% and 60% Ag.

In order to split into the trends followed by the elastic properties of Pd-Ag alloys, we introduce the following parameter:

TABLE I. Theoretical (EMTO-PBEsol) single and polycrystalline elastic constants and Debye temperature of Pd-Ag alloys as a function of Ag concentration.

at. %	c_{11} (GPa)	c_{12} (GPa)	c_{44} (GPa)	B (GPa)	G (GPa)	E (GPa)	ν	Θ (K)
0	234.08	189.95	112.75	204.66	59.56	162.88	0.367	315.74
10	221.84	177.49	111.75	192.27	59.32	161.37	0.360	313.50
20	209.58	165.87	108.96	180.44	58.06	157.31	0.355	308.60
30	198.68	155.63	105.07	169.98	56.41	152.37	0.351	302.73
40	189.20	146.55	100.02	160.77	54.47	146.82	0.348	296.12
45	185.35	141.67	97.11	156.23	53.91	145.06	0.345	293.85
50	182.07	136.77	93.97	151.87	53.52	143.67	0.342	292.04
55	177.78	132.40	90.19	147.53	52.19	140.05	0.342	287.71
60	171.60	128.79	85.71	143.06	49.46	133.04	0.345	279.57
65	166.44	126.18	82.15	139.60	47.07	126.94	0.348	272.32
70	160.91	122.84	78.37	135.53	44.76	120.96	0.351	265.03
80	150.58	117.16	71.51	128.30	40.26	109.35	0.358	250.38
90	140.62	111.37	65.49	121.12	36.27	98.92	0.364	236.49
100	132.99	106.26	61.38	115.17	33.68	92.07	0.367	226.90

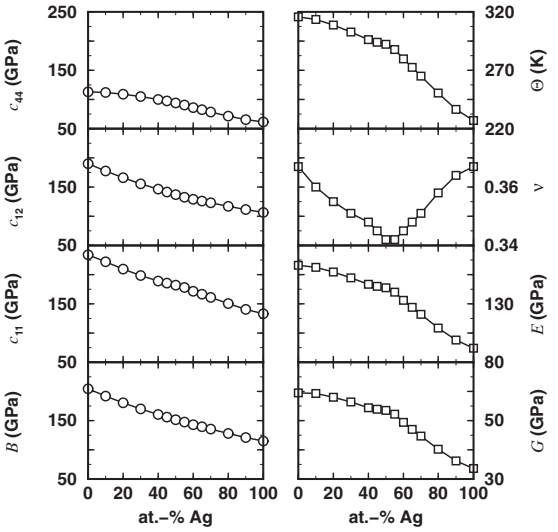

FIG. 4. Theoretical (EMTO-PBEsol) single and polycrystalline elastic constants and Debye temperature of Pd-Ag alloys as a function of Ag concentration.

$$\Delta C(x) \equiv C(x) - (1-x)C(\mathrm{Pd}) - xC(\mathrm{Ag}), \tag{5}$$

where $C(x)$ stands for a certain equilibrium property calculated for alloy with concentration x. By separating the "large" linear contribution $C_{\mathrm{lin}}(x) \equiv (1-x)C(\mathrm{Pd}) + xC(\mathrm{Ag})$ and the "small" nonlinear contribution $\Delta C(x)$, we can carry out a more detailed investigation of the alloying effects. Note that in the case of lattice constant, Eq. (5) describes the deviation relative to Vegard's rule, while in the case of total energy it corresponds to the mixing enthalpy.

The obtained relative deviations from the linear trend for the elastic properties are plotted in Fig. 5. The figure clearly shows that all single-crystal elastic constants deviate strongly

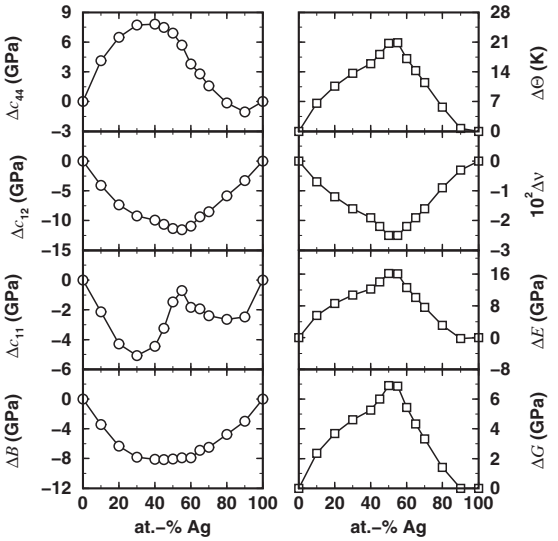

FIG. 5. Deviations from the linear behavior of the theoretical (EMTO-PBEsol) single and polycrystalline elastic constants and Debye temperature of Pd-Ag alloys as a function of Ag concentration.

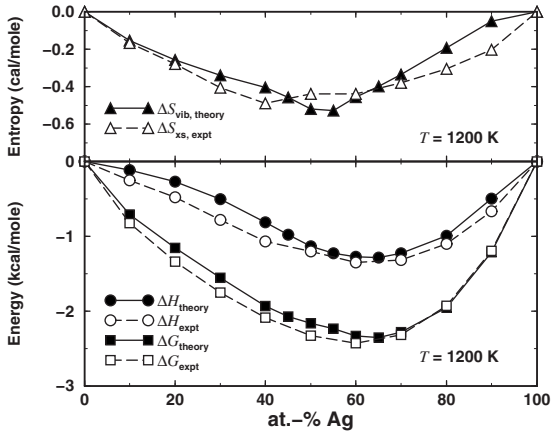

FIG. 6. Comparison between theoretical (present results) and experimental (Ref. 44) mixing enthalpy (ΔH), Gibbs energy of formation (ΔG), and excess entropy of formation (ΔS_{vib} and ΔS_{xs}) for Pd-Ag alloys as a function of Ag concentration. Both sets of data are for 1200 K, and the energy units refer to mole of atoms.

from the linear behavior (Fig. 5, left panels). The actual bulk modulus and $c_{12}(x)$ follow a nearly parabolic trend dropping by ~8–10 GPa relative to the linear $B_{\mathrm{lin}}(x)$ and $c_{12\ \mathrm{lin}}(x)$. On closer examination, we find that the first-order derivatives of $B(x)$ and $c_{12}(x)$ are discontinuous at ~30% and ~60% Ag. The other two elastic constants $c_{11}(x)$ and $c_{44}(x)$ display even more peculiar trends. $c_{44}(x)$ has a blurred breakpoint at $x=0.6$, and $\Delta c_{44}(x)$ changes sign around $x=0.8$. $c_{11}(x)$ has a double-minimum structure with a sharp first-order discontinuity between 50% and 60% Ag and a breakpoint at $x \approx 0.6$.

The strongly nonlinear trends in the single-crystal elastic constants are well reflected in the polycrystalline elastic moduli and Debye temperature (Fig. 5, right panels). The large positive deviations in $c_{44}(x)$ and $c'(x)=[c_{11}(x) - c_{12}(x)]/2$ (not shown) around the equimolar compositions yield large positive deviations for $G(x)$, $E(x)$, and $\Theta(x)$. On the other hand, the Poisson ratio exhibits a deep minimum (~0.34) near 55% Ag. This minimum shows that the corresponding alloys have larger G/B ratio compared to Pd-rich and Ag-rich alloys. Connecting the G/B ratio to the ductility of solids,[42] we find that the equimolar compositions are more brittle than the rest of the alloys.

The ~20 K maximum of $\Delta\Theta(x)$ near $x=0.55$ [representing ~7% of $\Theta(x)$] has important consequence on the phase diagram of Pd-Ag. To understand this effect, first we show that the present theory reproduces with high accuracy the formation energies of the Pd-Ag alloys. Putting the theoretical Debye temperatures from Table I into the Debye model (see, e.g., Refs. 43), we get the vibrational entropy of formation (ΔS_{vib}), which in turn can be compared to the experimental excess entropy of formation (ΔS_{xs}).[44] The agreement between the two sets of entropy from Fig. 6 (upper panel) can be considered very good, especially if we take into account the large error bar reported in experiments.[44] In the lower panel of Fig. 6, we compare the present enthalpy of formation (ΔH) and Gibbs energy of formation (ΔG) for temperature $T=1200$ K with the corresponding experimental data.[44] The theoretical Gibbs energy is obtained as ΔG

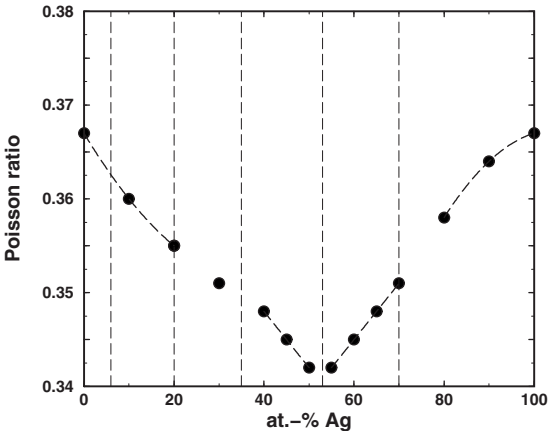

FIG. 7. Theoretical (EMTO-PBEsol) Poisson ratio for Pd-Ag alloys as a function of Ag concentration. The vertical dashed lines mark the positions of the ETTs predicted by the KKR calculation (Ref. 3).

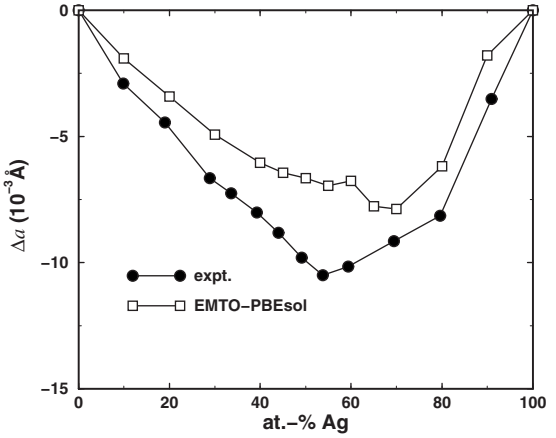

FIG. 8. Theoretical (EMTO-PBEsol) equilibrium lattice parameters for Pd-Ag alloys plotted relative to Vegard's rule as a function of Ag concentration. For completeness, the available experimental data (Ref. 1) are also shown.

$=\Delta H - T(\Delta S_{\text{vib}} + S_{\text{conf}})$, where the configurational entropy (S_{conf}) is calculated within the mean-field approximation, and the vibrational energy and entropy are estimated using the Debye model.[43] We find an excellent agreement between the theoretical and experimental formation energies, except for the Pd-rich alloys (containing ~60%–80% Pd) where the deviations are somewhat larger. The good correspondence between ΔH_{theory} and ΔH_{expt} demonstrates that, in contrast to what has been suggested in Ref. 22, the short-range-order effects in the enthalpy of formation of Pd-Ag are very small at temperatures around 1200 K. On the other hand, the negative excess entropy of formation (Fig. 6, upper panel) leads to a phonon free energy of mixing (not shown) that has a maximum around 55% Ag. Although at 1200 K this maximum is to a large extent washed out by the configurational entropy, its effect pops up as a negatively curved portion of ΔG_{theory} between ~45% and ~60% Ag, indicating segregation (spinodal decomposition) tendencies in the Pd-Ag system.

C. Discussion

Using a fully relativistic KKR method, Bruno *et al.*[3] found that there are five Fermi-surface topological transitions in random Pd-Ag alloys, and they occur near $x=0.06$, 0.20, 0.35, 0.53, and 0.70. They claimed that the equilibrium properties must show anomalies around the quoted concentrations. Indeed, our theoretical elastic constants from Figs. 4 and 5 display a series of peculiar features at concentrations $0.3 \lesssim x \lesssim 0.7$. To be more specific, in Fig. 7 we show the present Poisson ratio values and mark the critical concentrations of ETTs by Bruno *et al.*[3] In order to highlight the anomalies in the theoretical Poisson rations, we divide the calculated points in such a way that each small set of data can be fitted by a second-order polynomial (except the single point at $x=0.3$). In this way we can establish a good correspondence between the position of the anomalies (breakpoints in ν) and the ETTs.

However, the present calculations do not take into account the spin-orbit interaction, and therefore one cannot expect a perfect one-to-one correspondence between the elastic anomalies and the critical concentrations. The actual transitions are also blurred by the substitutional disorder.[3] A third factor that can make the comparison problematic is the way how the elastic constants are computed. Large numerical values for ε_o and ε_m in Eq. (4) make the ETT effects on $c_{ij}(x)$'s to be smeared within a finite concentration range around the critical concentration. Finally, due to the closeness of the ETTs, their effects overlap and lead to the rather complex trends in $c_{ij}(x)$. In spite of these difficulties, below we make an attempt to separate and understand the role of the main ETTs on the ground-state properties.

Our results for the equilibrium lattice parameters are plotted in Fig. 8. Starting from the Ag side, the lattice parameter decreases upon Pd addition showing a negative deviation relative to Vegard's rule. We make use of the expression for the pressure written within the atomic sphere approximation[45,46] to estimate the lattice contraction upon alloying. According to that, the total pressure is decomposed into a homogeneous positive *sp* pressure and a negative *d* pressure, viz.,

$$P_{\text{tot}}(V) = P_{sp}(n_{sp}/V) + P_d(n_d, V), \tag{6}$$

where n_{sp} and n_d denote the number of *sp* and *d* electrons, respectively, and V is the atomic volume. At equilibrium volume V_0 we have $P_{\text{tot}}(V_0)=0$. Equation (6) expresses the fact that the *sp* partial pressure depends on the average *sp* electron density, and the *d* partial pressure depends on the actual number of the *d* electrons and volume. Expanding the partial pressure around the equilibrium volume V_0 and using the expression for the bulk modulus ($B=V_0 \delta P_{\text{tot}}/\delta V$), one arrives to an expression which connects the volume change to the change in the occupation numbers. Following the procedure from Ref. 47, for the volume change we obtain

$$\frac{\Delta V}{V_0} \approx K \frac{\Delta n_{sp}}{n_{sp}}, \tag{7}$$

where $K=-V_0/Bn_d(10-n_d)\,\partial W/\partial V$ and W is the potential parameter describing the *d* bandwidth. The *d* bandwidth in-

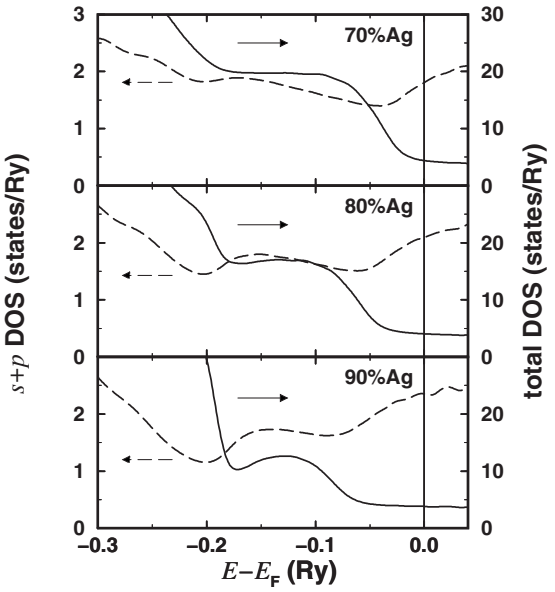

FIG. 9. Total (right axis) and partial *sp* (left axis) density of states for Pd-Ag alloys for 70%, 80%, and 90% Ag. The vertical lines mark the position of the Fermi level (E_F).

creases with pressure,[48] so we have $\partial W/\partial V<0$ and thus $K>0$. Therefore, according to Eq. (7), the volume change is proportional to the change in the *sp* occupation number, that is, a decrease in n_{sp} yields a negative ΔV.

The total and partial *sp* density of states (DOS) for 70%, 80%, and 90% Ag concentrations are shown in Fig. 9. Note that the partial *f* DOS is negligible in Pd-Ag system. With Pd addition (electron removal), corresponding to $-\Delta x=|\Delta x|$ change in the total number of electrons per atom, the Fermi level (E_F) is shifted to the left of the figure. Since in Ag-rich alloys the *d* band is far below the Fermi level, the *d* DOS is very small compared to the *sp* DOS at E_F (i.e., $\Delta n_d\approx 0$), and therefore the electrons are mainly removed from the *sp* band, which means that $\Delta n_{sp}\approx\Delta x$. In accordance with Eq. (7), this leads to a drop in the equilibrium volume proportional to $|\Delta x|$. This is in perfect agreement with Fig. 8.

In 90% alloy, the Fermi level is located on a local maximum of the *sp* DOS, and with increasing Pd amount, E_F is shifted toward lower *sp* DOS. At the same time, the *d* DOS at E_F slightly increases with Pd addition. Both of these effects result in $|\Delta n_{sp}|<|\Delta x|$ as x decreases from 0.9, and thus in a reduced volume change. That is why the volume drop between 80% and 60% Ag is much smaller compared to that between 90% and 80% (Fig. 8). Finally, when the Fermi level hits the *d* DOS (somewhere close to $x=0.6$), there is a sudden decrease in $|\Delta n_{sp}|$, since part of the electrons are now removed from the large *d* band. This results in a sudden decrease in $|\Delta V|$ around 60% Ag, in accordance with Fig. 8. We point out that the above changes in the equilibrium lattice parameter correlate well with the obtained changes in the bulk modulus (Fig. 5).

Returning to the electronic topological transitions, we recall that Bruno *et al.*[3] associated the topological transition at $x=0.53$ with the hole pockets centered at points *X* from the Brillouin zone. These pockets have *d* character. We suggest that this ETT is in fact the origin of the above-discussed sudden increase in the relative lattice parameter $\Delta a(x)$ (near $x=0.6$ in Fig. 8). Approaching the pockets from the Ag-rich side, around 60% Ag we start to deplete the *d* states around the *X* points, which yields an increase in $|\Delta n_d|$ (i.e., decrease in $|\Delta n_{sp}|\approx|\Delta x|-|\Delta n_d|$) and thus to the sharp increase in the equilibrium volume [decrease in $|\Delta a(x)|$].

IV. CONCLUSIONS

Using the EMTO-PBEsol approach we investigated the elastic properties of Pd-Ag random alloys. Our theoretical results provide the first consistent elastic parameter data for these alloys and call for systematic experimental studies on this important system. We have found that the variation in the elastic constants with concentration is not linear even though these alloys crystallize in a single fcc phase. In addition, the deviation from the linear change is found to follow a complex trend. Pronounced discontinuities in the first-order derivative as a function of Ag concentration are observed in the case of lattice constant, bulk modulus, c_{11} and c_{12} single-crystal elastic constants, and also in polycrystalline elastic moduli. Furthermore, these discontinuities are not found at the same Ag concentration for different parameters. In the case of lattice constant and bulk modulus the main discontinuities are located around 60% Ag, but in the case of c_{11} and c_{12} and the polycrystalline elastic moduli, the discontinuities are spread over a concentration range from ~30% to ~60% Ag. Using a model based on the partial pressures, we have presented a simple and transparent explanation for the main anomalies seen in the equilibrium lattice constant and bulk modulus.

ACKNOWLEDGMENTS

The Swedish Research Council, the Swedish Foundation for Strategic Research, the Swedish Energy Agency, the Carl Tryggers Foundation, the Academy of Finland (Grant No. 116317), and the Hungarian Scientific Research Fund (Grants No. T046773 and No. T048827) are acknowledged for financial support. The computer resources of the Finnish IT Center for Science (CSC) and Mgrid project are also acknowledged.

[1] W. B. Pearson, *A Handbook of Lattice Spacings and Structures of Metals and Alloys* (Pergamon, Oxford, 1958).

[2] E. Bruno, B. Ginatempo, and E. S. Giuliano, Phys. Rev. B **52**, 14544 (1995).

[3] E. Bruno, B. Ginatempo, and E. S. Giuliano, Phys. Rev. B **52**, 14557 (1995).

[4] I. M. Lifshitz, Zh. Eksp. Teor. Fiz. **33**, 1569 (1960) [Sov. Phys. JETP **11**, 1130 (1960)].

[5] O. K. Andersen, O. Jepsen, and G. Krier, *Lectures on Methods of Electronic Structure Calculation* (World Scientific, Singapore, 1994), p. 63.
[6] L. Vitos, H. L. Skriver, B. Johansson, and J. Kollár, Comput. Mater. Sci. **18**, 24 (2000).
[7] L. Vitos, Phys. Rev. B **64**, 014107 (2001).
[8] L. Vitos, I. A. Abrikosov, and B. Johansson, Phys. Rev. Lett. **87**, 156401 (2001).
[9] L. Vitos, in *Computational Quantum Mechanics for Materials Engineers* (Springer-Verlag, London, 2007).
[10] P. Hohenberg and W. Kohn, Phys. Rev. **136**, B864 (1964).
[11] W. Kohn and L. J. Sham, Phys. Rev. **140**, A1133 (1965).
[12] A. Taga, L. Vitos, B. Johansson, and G. Grimvall, Phys. Rev. B **71**, 014201 (2005).
[13] Z. Nabi, L. Vitos, B. Johansson, and R. Ahuja, Phys. Rev. B **72**, 172102 (2005).
[14] L. Vitos, P. A. Korzhavyi, and B. Johansson, Nature Mater. **2**, 25 (2003).
[15] B. Magyari-Köpe, G. Grimvall, and L. Vitos, Phys. Rev. B **66**, 064210 (2002); **66**, 179902(E) (2002).
[16] B. Magyari-Köpe, L. Vitos, and G. Grimvall, Phys. Rev. B **70**, 052102 (2004).
[17] L. Vitos, P. A. Korzhavyi, and B. Johansson, Phys. Rev. Lett. **88**, 155501 (2002).
[18] L. Huang, L. Vitos, S. K. Kwon, B. Johansson, and R. Ahuja, Phys. Rev. B **73**, 104203 (2006).
[19] J. P. Perdew, A. Ruzsinszky, G. I. Csonka, O. A. Vydrov, G. E. Scuseria, L. A. Constantin, X. Zhou, and K. Burke, Phys. Rev. Lett. **100**, 136406 (2008).
[20] M. Ropo, K. Kokko, and L. Vitos, Phys. Rev. B **77**, 195445 (2008).
[21] *Binary Alloy Phase Diagrams*, edited by T. B. Massalski (ASM International, Metals Park, OH, 1992).
[22] S. Müller and A. Zunger, Phys. Rev. Lett. **87**, 165502 (2001).
[23] A. V. Ruban, S. I. Simak, P. A. Korzhavyi, and B. Johansson, Phys. Rev. B **75**, 054113 (2007).
[24] G. Grimvall, *Thermophysical Properties of Materials: Enlarged and Revised Edition* (North-Holland, Amsterdam, 1999).
[25] J. A. Rayne, Phys. Rev. **118**, 1545 (1960).
[26] J. Ashkenazi, M. Dacorogna, M. Peter, Y. Talmor, E. Walker, and S. Steinemann, Phys. Rev. B **18**, 4120 (1978).
[27] P. Soven, Phys. Rev. **156**, 809 (1967).
[28] B. L. Gyorffy, Phys. Rev. B **5**, 2382 (1972).
[29] J. Kollár, L. Vitos, and H. L. Skriver, in *Electronic Structure and Physical Properties of Solids: The Uses of the LMTO Method*, Lecture Notes in Physics, edited by H. Dreyssé (Springer-Verlag, Berlin, 2000), p. 85.
[30] O. K. Andersen, C. Arcangeli, R. W. Tank, T. Saha-Dasgupta, G. Krier, O. Jepsen, and I. Dasgupta, in Mater. Res. Soc. Symp. Proc. **491**, 3 (1998).
[31] P. A. Korzhavyi, A. V. Ruban, I. A. Abrikosov, and H. L. Skriver, Phys. Rev. B **51**, 5773 (1995).
[32] F. D. Murnaghan, Proc. Natl. Acad. Sci. U.S.A. **30**, 244 (1944).
[33] J. P. Perdew and Y. Wang, Phys. Rev. B **45**, 13244 (1992).
[34] J. P. Perdew, K. Burke, and M. Ernzerhof, Phys. Rev. Lett. **77**, 3865 (1996).
[35] L. Vitos, B. Johansson, J. Kollár, and H. L. Skriver, Phys. Rev. B **62**, 10046 (2000).
[36] R. Armiento and A. E. Mattsson, Phys. Rev. B **72**, 085108 (2005).
[37] M. Asato, A. Settels, T. Hoshino, T. Asada, S. Blügel, R. Zeller, and P. H. Dederichs, Phys. Rev. B **60**, 5202 (1999).
[38] C. Kittel, *Introduction to Solid State Physics*, 7th ed. (Wiley, New York, 1996).
[39] H. H. Kart, M. Tomak, M. Ulugogan, and T. Cagin, Comput. Mater. Sci. **32**, 107 (2005).
[40] F. Jona and P. M. Marcus, Phys. Rev. B **65**, 155403 (2002).
[41] P. Söderlind, O. Eriksson, J. M. Wills, and A. M. Boring, Phys. Rev. B **48**, 5844 (1993).
[42] S. F. Pugh, Philos. Mag. **45**, 823 (1954).
[43] K. Kádas, L.Vitos, B. Johansson, and J. Kollár, Phys. Rev. B **75**, 035132 (2007).
[44] R. Hultgren *et al.*, *Selected Values of the Thermodynamic Properties of Binary Alloys* (American Society for Metals, Metals Park, Ohio, 1973).
[45] O. K. Andersen, Solid State Commun. **13**, 133 (1973).
[46] D. G. Pettifor, J. Phys. F: Met. Phys. **8**, 219 (1978).
[47] K. Kádas, Z. Nabi, S. K. Kwon, L. Vitos, R. Ahuja, B. Johansson, and J. Kollár, Surf. Sci. **600**, 395 (2006).
[48] O. K. Andersen, O. Jepsen, and D. Glötzel, in *Highlights of Condensed Matter Theory*, edited by F. Bassani, F. Fumi, and M. P. Tosi (North-Holland, New York, 1985), p. 59.